Inorganica Chimica Acta 370 (2011) 427–434

Contents lists available at ScienceDirect

Inorganica Chimica Acta

journal homepage: www.elsevier.com/locate/ica

Synthesis, crystal structures, electrochemical and magnetic properties of polynuclear $\{Fe_4\}$ and $\{Fe_8Na_4\}$ carboxylate/picolinate clusters

L. Arizaga [a], M.F. Cerdá [b], R. Faccio [c], A.W. Mombrú [c], M.A. Novak [d], R. González [a], C. Kremer [a], R. Chiozzone [a,*]

[a] Cátedra de Química Inorgánica, Departamento "Estrella Campos", Facultad de Química, CC 1157, Montevideo, Uruguay
[b] Laboratorio de Biomateriales, Facultad de Ciencias, Universidad de la República, Iguá 4225, Montevideo, Uruguay
[c] Laboratorio de Cristalografía, DETEMA, Facultad de Química, CC 1157, Montevideo, Uruguay
[d] Instituto de Física, Universidade Federal do Río de Janeiro, Brazil

ARTICLE INFO

Article history:
Received 8 September 2010
Received in revised form 1 February 2011
Accepted 9 February 2011
Available online 16 February 2011

Keywords:
Iron(III) carboxylate clusters
Iron(III) picolinate complexes
Electrochemical properties
Magnetic properties

ABSTRACT

Reaction of sodium picolinate with Fe^{III} oxo-centered carboxylate triangles in MeCN in the presence of PPh_4Cl yields $(PPh_4)[Fe_4O_2(O_2CR)_7(pic)_2]$ (R = Ph (**1**), Bu^t (**2**)). Omitting the phosphonium cation produces $[Fe_8Na_4O_4(O_2CPh)_{16}(pic)_4(H_2O)_4]$ (**3**), which contains two Fe_4Na_2 units bridged by two picolinate ligands. X-ray crystal structures of **1** and **3** are reported.

Voltammetric profiles in MeCN show four one-electron reduction steps for complexes **1** and **2**. Variable-temperature magnetic susceptibility measurements in polycrystalline samples of **1** and **3** reveal strong antiferromagnetic couplings leading to $S = 0$ ground states.

© 2011 Elsevier B.V. All rights reserved.

1. Introduction

Polynuclear Fe^{III} compounds with oxygen donor ligands have received a great attention mainly due to their relevance in bioinorganic chemistry and in molecular magnetism. Iron-oxo and -hydroxo complexes have been studied as synthetic models of the active sites of various non-heme metalloenzymes, such as hemerythrin and ribonucleotide reductase [1], and as model systems for iron storage proteins, as ferritin [2]. In addition, some iron clusters can possess large total spin values in their ground state, and can even behave occasionally as single-molecule magnets (SMMs) [3], which is relevant to the field of molecular magnetic materials. SMMs are molecules that can function as single-domain magnetic particles of nanoscale dimensions, exhibit a slow relaxation rate of the magnetization, and present magnetic hysteresis below a certain blocking temperature [4].

The exchange interactions between Fe^{III} centers within multinuclear iron-oxo or -hydroxo clusters $\{Fe_x\}$ are normally antiferromagnetic. However, in some $\{Fe_x\}$ topologies, large spin ground states can arise even when all the pairwise Fe_2 interactions are antiferromagnetic because of the occurrence of competing exchange interactions that frustrate the preferred spin alignments [5]. Nuclearity and topology of the polynuclear metal complexes depend strongly on the ligands that complete the peripheral coordination of the cluster, acting as bridging or chelating terminal groups. In this respect, the ligand blend RCO_2^-/L–L (L–L = bidentate ligand) have been intensely studied and several Fe_x cluster types have been reported [6]. When L–L = picolinate (pic, the anion of the 2-pyridinecarboxylic acid), the up to now structurally characterized members of this family are $[NBu_4][Fe^{III}_4O_2(O_2CMe)_7(pic)_2]$ [7], $[Fe^{II}Fe^{III}_3O_2(O_2CBu^t)_7(Hpic)_{1.5}(Kpic)_{0.5}]$ [8] and $[Fe^{III}_6Na_2O_2(O_2CPh)_{10}(pic)_4(EtOH)_4(H_2O)_2](ClO_4)$ [9]. The first two of them have the well-documented bent ("butterfly") arrangement of four iron sites in $[Fe_4(\mu_3\text{-}O)_2]$ units, while the third consists of two symmetry-related $[Fe_3O]$ triangles.

We have thus revisited the reaction system consisting of Fe^{III} and RCO_2^-/picolinate, and tried to investigate the effects of a change in the carboxylate ligand or in the counterion on the nuclearity and/or the topology of the iron cage. In this paper, we describe the synthesis and characterization of complexes $(PPh_4)[Fe_4O_2(O_2CR)_7(pic)_2]$ (R = Ph (**1**), Bu^t (**2**)) and $[Fe_8Na_4O_4(O_2CPh)_{16}(pic)_4(H_2O)_4]$ (**3**). The electrochemical properties of compounds **1** and **2** in acetonitrile solution are reported. In addition, we also present X-ray crystal structures and magnetic properties of **1** and **3**.

2. Experimental

2.1. General procedure

All chemicals were of reagent grade and used as received. $Na(pic)\cdot 3/4H_2O$ was prepared from picolinic acid (Hpic) and NaOH as described [10]. $[Fe_3O(O_2CPh)_6(H_2O)_3](O_2CPh)$ was prepared

* Corresponding author. Tel.: +598 2924 9739; fax: +598 2924 1906.
E-mail address: rchiozzo@fq.edu.uy (R. Chiozzone).

0020-1693/$ - see front matter © 2011 Elsevier B.V. All rights reserved.
doi:10.1016/j.ica.2011.02.021

from $FeCl_3{\cdot}6H_2O$ and benzoic ($PhCO_2H$) acid following the literature procedures [11]. $[Fe_3O(O_2CBu^t)_6(H_2O)_3]Cl{\cdot}H_2O$ was obtained similarly but starting from pivalic acid (Bu^tCO_2H) (*Anal.* Calc. for $C_{30}H_{60}Fe_3ClO_{16}{\cdot}H_2O$: C, 40.1; H, 7.0. Found: C, 40.0; H, 7.2%).

Infrared spectra were recorded with a Bomen MB 102 FTIR spectrophotometer as KBr pellets in the 4000–200 cm^{-1} region. Elemental analysis was accomplished on a Carlo Erba model 1108 elemental analyzer. The negative-ion ESI mass spectra of **1** and **2** in MeCN solution were performed using a Q-TOF (Bruker Daltoniks) mass spectrometer equipped with an ESI source.

The voltammetric profile of 1 mM solutions of compounds **1** and **2** was evaluated in MeCN with 0.04 M NEt_4ClO_4 as supporting electrolyte. Measurements were carried out in a one-compartment conic cell, using a polycrystalline (*pc*) Au disk (3 mm diameter) as working electrode, a Pt sheet as counter electrode and an Ag/$AgNO_3$ 0.1 M in the supporting electrolyte (E = 0.60 V versus NHE) as the reference. All potentials in the text are referred to NHE. Voltammograms were obtained at potential scan rates v within the range 0.0025 V $s^{-1} \leqslant v \leqslant$ 0.050 V s^{-1}.

The magnetic measurements on polycrystalline samples of **1** and **3** were carried out with a Cryogenics SX600 SQUID magnetometer in the temperature range 2.4–300 K and under an applied magnetic field of 0.0960 T. The device was calibrated with YFeGarnet NIST reference samples. Diamagnetic corrections of the constituent atoms were estimated from Pascal's constants.

2.1.1. Synthesis of $(PPh_4)[Fe_4O_2(O_2CPh)_7(pic)_2]{\cdot}2H_2O$ (**1**·$2H_2O$)

To a stirred suspension of $[Fe_3O(O_2CPh)_6(H_2O)_3](O_2CPh)$ (218 mg, 0.2 mmol) and PPh_4Cl (143 mg, 0.38 mmol) in MeCN (10 mL) was slowly added a solution of $Na(pic){\cdot}3/4H_2O$ (60 mg, 0.38 mmol) in H_2O (0.20 mL). The brown solution was allowed to evaporate very slowly, producing prismatic amber crystals of **1**·$2H_2O$ in ~50% yield over the course of 10 days. The solid was filtered off, washed with few drops of cold MeCN and dried in vacuo over silica gel. X-ray quality crystals were obtained directly from the mother liquors. Selected IR data [KBr, ν_{max}/cm^{-1}] 1669m, 1597s, 1557s, 1539s, 1397vs, 1349m, 1292m, 1174m, 1024m, 851m, 718s, 471s, 337m. *Anal.* Calc. for $C_{85}H_{63}Fe_4PN_2O_{20}{\cdot}2H_2O$: C, 59.3; H, 3.9; N, 1.6. Found: C, 59.2; H, 4.2; N, 1.7%.

2.1.2. Synthesis of $(PPh_4)[Fe_4O_2(O_2CBu^t)_7(pic)_2]{\cdot}2H_2O$ (**2**·$2H_2O$)

Compound **2**·$2H_2O$ was prepared in ~30% yield by a similar procedure, but starting from $[Fe_3O(O_2CBu^t)_6(H_2O)_3]Cl{\cdot}H_2O$ (177 mg, 0.20 mmol). Selected IR data [KBr, ν_{max}/cm^{-1}] 1656m, 1580s, 1543m, 1483s, 1417s, 1374m, 1361m, 1227m, 852m, 690m, 604m, 436m. *Anal.* Calc. for $C_{71}H_{91}Fe_4PN_2O_{20}{\cdot}2H_2O$: C, 53.9; H, 6.0; N, 1.8. Found: C, 53.7; H, 6.2; N, 1.8%.

2.1.3. Synthesis of $[Fe_8Na_4O_4(O_2CPh)_{16}(pic)_4(H_2O)_4]{\cdot}MeCN{\cdot}9H_2O$ (**3**·$MeCN{\cdot}9H_2O$)

To a stirred suspension of $[Fe_3O(O_2CPh)_6(H_2O)_3](O_2CPh)$ (218 mg, 0.2 mmol) in MeCN (10 mL) was slowly added a solution of $Na(pic){\cdot}3/4H_2O$ (60 mg, 0.38 mmol) in H_2O (0.20 mL). The solution was left undisturbed for 24 h, producing dark red crystals of **3**·$MeCN{\cdot}9H_2O$ in ~40% yield. The solid was filtered off, washed with MeCN and dried in vacuo over silica gel. X-ray quality crystals could be obtained directly from the mother liquor. This compound can not be redissolved in MeCN and the drained-out solid is very sensitive to air. Selected IR data [KBr, ν_{max}/cm^{-1}] 1599s, 1561s, 1541sh, 1405vs, 1357m, 1175m, 1025m, 718s, 675m, 468s. Dried solid analyzed as **3**·$4H_2O$ (*Anal.* Calc. for $C_{136}H_{104}Na_4Fe_8N_4O_{48}{\cdot}4H_2O$: C, 51.5; H, 3.6; N, 1.8. Found: C, 51.9; H, 3.4; N, 1.9%).

2.2. X-ray data collection and structure refinement

The X-ray diffraction data for **1** was collected at 293(2) K with an RIGAKU AFC-7S four-circle diffractometer [12] using graphite monochromatized Mo Kα radiation (λ = 0.71069 Å) in the $\theta/2\theta$ scan mode. In the case of compound **3**, a Bruker APEXII CCD difractometer was used, equiped with graphite monochromatic Mo Kα radiation operating in a ω scan mode. Crystal data, collection procedures and refinement results are summarized in Table 1. In the case of complex **1**, absorption and intensity decay corrections were applied to the diffraction data due to the observation of a significant crystal damaging during data collection. The final residuals indicate the existence of a number of reflections poorly fitted, and bond lengths and angles show a slightly high standard deviation as a consequence of the mentioned problem. Both structures were solved by direct methods locating most of the non-H atoms using SHELXS [13]. Fourier recycling and least-squares refinement were used for model completion with SHELXL [13] included in the WINGX suite of programs [14]. All non-H atoms have been refined anisotropically, and all H atoms have been placed in geometrically suitable positions and refined riding with isotropic thermal parameter related to the equivalent isotropic thermal parameter of the parent atom. The geometrical analysis of interactions in the structures was performed with PLATON [15].

Many voids appear in the structure of **3** as potential sites for further solvent location. All these sites were evaluated, finding a disordered CH_3CN molecule sharing this region with one water molecule represented by O(7w) which presents half site occupancy. For this reason both, O(7w) and CH_3CN molecule were refined isotropically with the same displacement parameters for C and N atoms in MeCN. Finally, other four oxygen atoms from non coordinated water molecules were identified and fully refined.

Table 1
Crystallographic data and structure refinements for **1**·$2H_2O$ and **3**·$MeCN{\cdot}9H_2O$.

Cristal data	**1**·$2H_2O$	**3**·$MeCN{\cdot}9H_2O$
Formula	$C_{85}H_{63}Fe_4PN_2O_{20}{\cdot}2H_2O$	$C_{136}H_{104}Na_4Fe_8N_4O_{48}{\cdot}H_3C_2N{\cdot}9H_2O$
Formula weight	287.13	3302.18
Crystal system	monoclinic	triclinic
Space group	$P2/n$	$P\bar{1}$
a (Å)	14.563(12)	14.236(3)
b (Å)	18.876(5)	14.601(3)
c (Å)	15.019(8)	19.320(4)
α (°)	90	85.22(3)
β (°)	105.21(4)	86.73(3)
γ (°)	90	65.83(3)
V (Å^3)	3984(4)	3649.9(16)
Z	2	1
D_{calc} (g/cm^3)	1.436	1.502
μ(Mo Kα) (mm^{-1})	0.81	0.877
F(0 0 0)	1772	1694
Crystal size (mm)	0.20 × 0.20 × 0.40	0.03 × 0.17 × 0.18
Data collection		
Temperature (K)	293	296
Radiation [Å]	0.71073	0.71073
Theta minimum–maximum (°)	2.0, 27.5	1.5, 25.0
Dataset	0:18; −4:24; −19:18	−16:16; −17:17; −22:18
Tot., Uniq. Data, $R_{(int)}$	12148, 9135, 0.080	57909, 12802, 0.045
Observed data [I > 2.0 sigma(I)]	5049	8957
Refinement		
N_{ref}, N_{par}	9135, 524	12,802,988
R, wR^2, S	0.0861, 0.2984, 1.07	0.0447, 0.1105, 1.03

$w = 1/[\sigma^2(F_o^2) + (0.0461P)^2 + 3.4901P]$ where $P = (F_o^2 + 2F_c^2)/3$

All of them presented full site occupancy. Hydrogen atoms from the disordered MeCN molecule were positioned using two idealized methyl positions. On the other hand, hydrogen atoms from water molecules were not included in the model due to difficulties appeared during the refinement.

2.3. Computational details

The theoretical study of $[Fe_4O_2(O_2CPh)_7(pic)_2]^-$ ion was based on First Principles – Density Functional Theory [16,17]. The simulations were performed using the SIESTA code [18–20] which adopts a linear combination of numerical localized atomic-orbital basis sets for the description of valence electrons and norm-conserving non-local pseudopotentials for the atomic core. The pseudopotentials were constructed using the Trouiller and Martins scheme [21] which describes the interaction between the valence electrons and atomic core. We selected a split-valence double-ζ basis set with polarization orbitals for all the carbon atoms. The extension of the orbitals is determined from a confinement, using an energy shift of 50 meV due to the localization. The total energy was calculated within the Perdew–Burke–Ernzerhof (PBE) form of the generalized gradient approximation GGA xc-potential [22]. The real-space grid used to represent the charge density and wavefunctions was the equivalent of that obtained from a plane-wave cutoff of 600 Ry. The atomic positions were kept fixed at the experimental crystallographic coordinates. Since the model was elaborated for an isolated ion, only Gamma-point was used to sample the full Brillouin Zone. All these parameters allowed the convergence of the total energy, which corresponded to the antiferromagnetic solution in all the cases.

3. Results and discussion

3.1. Synthesis

Compounds **1** and **2** were obtained in good yield in a single step from $[Fe_3O(O_2CR)_6(H_2O)_3]^+$ (R = Ph, Bu^t), pic^- and PPh_4Cl in MeCN:

$$4/3[Fe_3O(O_2CR)_6(H_2O)_3]X + 2Napic + PPh_4Cl \rightarrow (PPh_4)[Fe_4O_2(O_2CR)_7(pic)_2] + RCOOH + NaCl + NaX + 1/3HX + 10/3H_2O \quad (1)$$

The preparation of the NBu_4^+ salts of $[Fe_4O_2(O_2CR)_7(pic)_2]^-$ with R = Me and Ph, has been reported some years ago by Christou and co-workers [7], but they were synthesized by a different method and only the crystal structure of the acetate compound was described.

Single crystals of **2** suitable for X-ray analysis were not obtained, and for this reason its magnetic properties were not measured. This compound was formulated as the pivalate analog of **1** on the basis of elemental analyses and for comparison of the ESI(−) mass spectrum of both complexes in MeCN solution. The most intense fragments $[Fe^{II}_2Fe^{III}_2O_2(O_2CPh)_7(pic)_2+2H]^-$ (in the spectrum of **1**) and $[Fe^{II}_2Fe^{III}_2O_2(O_2CBu^t)_7(pic)_2+2H]^-$ (in the spectrum of **2**) were detected centered at *m*/*z* 1349 and 1209, respectively. This assignment is consistent with the fact that Fe^{III} species are easily reduced in negative ion mode [23] and also with the electrochemical behavior of both compounds in MeCN described in Section 3.3.

Complex **3** is structurally related to **1** in that also contains analogous butterfly-type Fe_4 cores. However, sodium atoms are incorporated not only balancing charges, but also altering the coordination modes of the ligands and making possible an increase in the nuclearity. The change of PPh_4^+ for Na^+ as counterion provokes the formation of a different architecture in the crystalline product.

IR spectra are characterized by several strong bands in the 1540–1670 cm^{-1} and 1340–1420 cm^{-1} regions, assigned to the ν_{as}(COO) and ν_s(COO) modes of the carboxylate ligands, respectively. However, due to the existence of different carboxylate groups and their coordination modes in each molecule, a more detailed band assignment has not been intended.

3.2. Description of the structures

Perspective drawings of the structures of compounds **1** and **3** showing the atom numbering are depicted in Figs. 1 and 2,

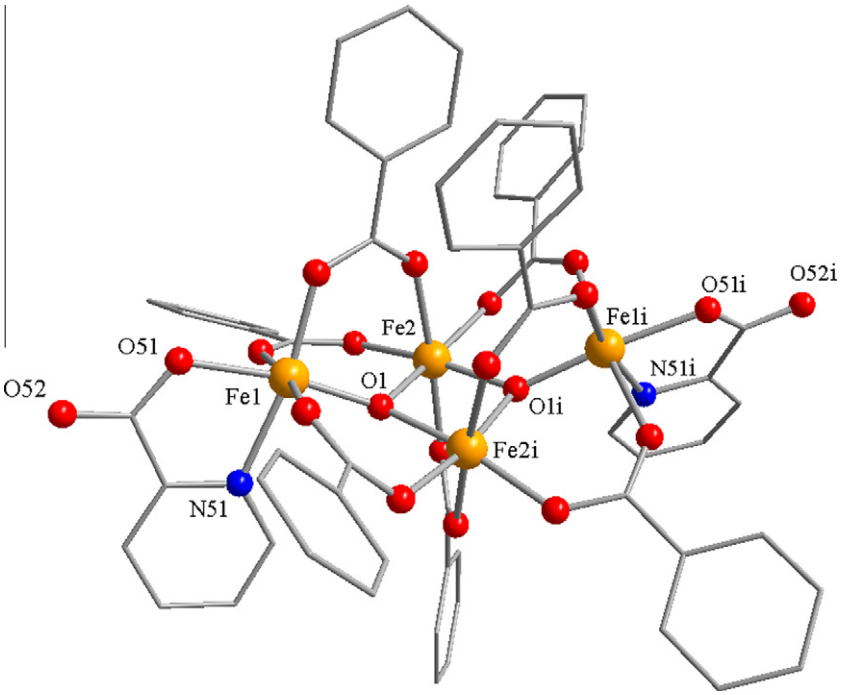

Fig. 1. Structure of the anion of **1**, with the hydrogen atoms ommited for clarity. The symmetry related atoms were obtained applying the symmetry code *i* = 0.5 − *x*, *y*, 1.5 − *z*. Color code: Fe yellow, O red, N blue, C gray. (For interpretation of the references to color in this figure legend, the reader is referred to the web version of this article.)

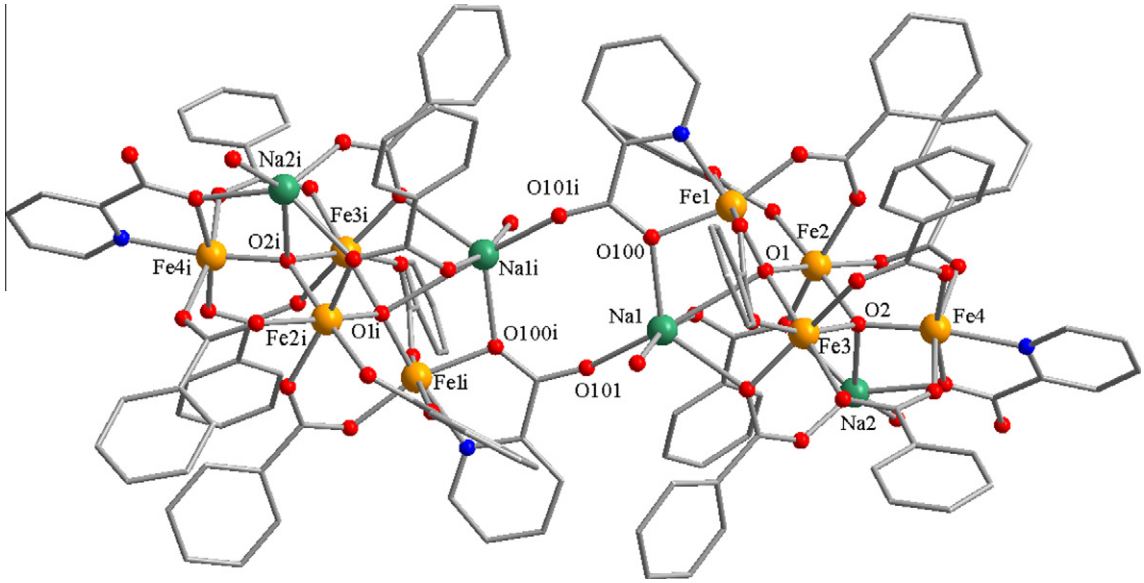

Fig. 2. The molecular structure of $[Fe_8Na_4O_4(O_2CPh)_{16}(pic)_4(H_2O)_4]$ (**3**), with hydrogen atoms ommited for clarity. The symmetry related atoms were obtained applying the symmetry code $i = -x, 1-y, -z$. Color code: Fe yellow, Na green, O red, N blue, C gray. (For interpretation of the references to color in this figure legend, the reader is referred to the web version of this article.)

Table 2
Selected interatomic distances (Å) and angles (°) for complex **1**·2H$_2$O.

Bond distances (Å)			
Fe(1)–O(1)	1.840(3)	Fe(2)–O(1)	1.918(4)
Fe(1)–O(22)	1.985(4)	Fe(2)–O(11)	2.068(4)
Fe(1)–O(31)	2.074(5)	Fe(2)–O(21)	2.070(4)
Fe(1)–O(42)	2.054(5)	Fe(2)–O(41)	2.010(4)
Fe(1)–O(51)	2.030(4)	Fe(2)–O(1)^{i}	1.940(4)
Fe(1)–N(51)	2.177(5)	Fe(2)–O(32)^{i}	2.028(5)
Selected angles (°)			
Fe(1)–O(1)–Fe(2)	123.8(2)		
Fe(2)–O(1)–Fe(2)^{i}	95.19(14)		
Fe(1)–O(1)–Fe(2)^{i}	134.0(2)		
O(1)–Fe(1)–O(22)	95.90(17)	O(1)–Fe(2)–O(11)	89.37(15)
O(1)–Fe(1)–O(31)	92.52(19)	O(1)–Fe(2)–O(21)	88.22(15)
O(1)–Fe(1)–O(42)	93.76(19)	O(1)–Fe(2)–O(41)	98.34(16)
O(1)–Fe(1)–O(51)	170.98(16)	O(1)–Fe(2)–O(1)^{i}	84.42(16)
O(1)–Fe(1)–N(51)	94.27(16)	O(1)–Fe(2)–O(32)^{i}	169.52(16)
Metal to metal distances (Å)			
Fe(1)···Fe(2)	3.315(2)		
Fe(2)···Fe(2)^{i}	2.849(3)		
Fe(1)···Fe(2)^{i}	3.480(2)		

Symmetry code: i = ½ − *x*, *y*, 3/2 − *z*.

Table 3
Selected hydrogen bonds [Å and °] for complex **1**·2H$_2$O.

D–H···A	D–H (Å)	H···A (Å)	D···A (Å)	D–H···A (°)
Ow1–Hw1···O52^{ii}	0.91(7)	2.06(7)	2.874(8)	148(6)
Ow1–Hw2···O51^{i}	0.90(7)	2.10(7)	2.994(9)	173(6)

Symmetry transformations used to generate equivalent atoms: ii = *x*, *y*, 1 + *z* and i = ½ − *x*, *y*, 3/2 − *z*.

respectively. Selected bond lengths and angles are summarized in Tables 2 and 4.

Compound **1**·2H$_2$O crystallizes in the centrosymmetric monoclinic space group *P*2/*n*. Its structure consists of discrete $[Fe_4O_2(O_2CPh)_7(pic)_2]^-$ anions, PPh_4^+ cations and water molecules. Each anion displays C_2 symmetry and contains a "butterfly" tetranuclear $[Fe_4(\mu_3\text{-}O)_2]^{8+}$ core. Fe(2) and Fe(2i) are located along the "body" of the butterfly, while the other two, Fe(1) and Fe(1i) are positioned at the tip of the "wings" [(i) = 0.5 − *x*, *y*, 1.5 − *z*]. The Fe_3 wings are bridged by pyramidal μ_3-O^{2-} ions (O(1) and O(1i) atoms). These ions lie out of the plane of the Fe_3 triangles by 0.280(3) Å, and are on the same side of the non planar Fe_4 rhombus (Type I conformation). The sum of the Fe–O–Fe angles around the μ_3-O^{2-} group is 353.1(2)°. The dihedral angle between the two Fe_3 planes is 145.28(3)°.

Six carboxylate groups from benzoate bridge the body-wingtip Fe_2 pairs in its common *syn*, *syn* μ_2-binding mode or 2.11 using Harris notation [24] and a seventh carboxylate bridges the hinge Fe atoms. Six-coordinated, near-octahedral geometry at each Fe^{III} is completed by two terminal picolinate chelate groups attached to the wingtip Fe centers.

The O(52) atom, from the carboxylic group of the picolinate, is free to act as hydrogen bond acceptor with water molecules. Also, the O(51) atom from pic^- which is bonded to Fe(1) participates in a slightly weaker hydrogen bond. Both connect the Fe_4 clusters, establishing an infinite chain along the [0 0 1] crystallographic direction (Fig. S1). All the relevant hydrogen bonds parameters are listed in Table 3.

Compound **3**·MeCN·9H$_2$O crystallizes in the triclinic space group $P\bar{1}$. The structure consists of neutral dodecanuclear $\{Fe_8Na_4\}$ entities and solvent molecules. Two picolinate ligands, both bridging in a $3.2_{12}1_31_1$ mode (Scheme 1), hold together two equivalent $\{Fe_4Na_2(\mu_4\text{-}O)_2(O_2CPh)_8(pic)(H_2O)_2\}$ subunits related by an inversion center (Fig. 3). In this way, the shortest distance between Fe atoms located in these separated fragments is 8.729(3) Å for Fe(1)···Fe(1i) [(i) = −*x*, 1 − *y*, −*z*]. The four Fe^{III} atoms in each subunit belong to a similar, but not identical core to that of **1**, with Fe(2) and Fe(3) along the body connected by two oxygen bridges to Fe(1) and Fe(4) at the wingtips. However, in this case the bridges are tetrahedral μ_4-O^{2-} ions, the fourth position being occupied by Na^I ions. The sum of the Fe–O–Fe angles around the μ_4-O^{2-} groups are 347.0(1)° for O(1) and 346.5(1)° for O(2), and the dihedral angle between the two Fe_3 planes is 139.12(3)°.

The Na atoms also modify the arrangement of the peripheral ligands around the metal cage in each subunit. Six benzoate groups bridge the body-wingtip Fe_2 pairs, but there are two other benzoate ligands binding in a 3.21 mode that bridge each body iron with

Table 4
Selected interatomic distances (Å) and angles (°) for complex **3**·MeCN·9H_2O.

Bond distances (Å)					
Fe(1)–O(1)	1.852(2)	Fe(3)–O(1)	1.967(2)	Na(1)–O(1)	2.814(3)
Fe(1)–O(11)	2.023(3)	Fe(3)–O(2)	1.939(2)	Na(1)–O(1w)	2.370(4)
Fe(1)–O(31)	2.034(2)	Fe(3)–O(10)	2.062(3)	Na(1)–O(21)	2.485(3)
Fe(1)–O(60)	2.016(2)	Fe(3)–O(21)	2.009(3)	Na(1)–O(41)	2.343(3)
Fe(1)–O(100)	2.022(2)	Fe(3)–O(71)	2.100(3)	Na(1)–O(100)	2.349(3)
Fe(1)–N(100)	2.170(3)	Fe(3)–O(81)	2.015(2)	Na(1)–O(101)	2.262(3)
Fe(2)–O(1)	1.924(2)	Fe(4)–O(2)	1.856(2)	Na(2)–O(2)	2.595(3)
Fe(2)–O(2)	1.977(2)	Fe(4)–O(51)	2.056(2)	Na(2)–O(3w)	2.284(5)
Fe(2)–O(30)	2.024(2)	Fe(4)–O(70)	2.006(3)	Na(2)–O(20)	2.212(3)
Fe(2)–O(40)	2.023(3)	Fe(4)–O(80)	2.037(2)	Na(2)–O(40)	2.334(3)
Fe(2)–O(50)	2.047(3)	Fe(4)–O(90)	2.021(3)	Na(2)–O(90)	2.295(3)
Fe(2)–O(61)	2.073(3)	Fe(4)–N(90)	2.191(3)		
Selected angles (°)					
Fe(1)–O(1)–Fe(2)	119.85(12)				
Fe(2)–O(1)–Fe(3)	97.09(11)				
Fe(1)–O(1)–Fe(3)	130.08(14)				
Fe(3)–O(2)–Fe(4)	122.11(13)				
Fe(2)–O(2)–Fe(3)	96.26(11)				
Fe(2)–O(2)–Fe(4)	128.08(13)				
Metal to metal distances (Å)					
Fe(1)···Fe(2)	3.268(2)	Fe(1)···Fe(1)^{i}	8.729(3)		
Fe(1)···Fe(3)	3.462(2)	Fe(1)···Fe(2)^{i}	9.912(3)		
Fe(1)···Fe(4)	5.706(3)	Fe(1)···Fe(3)^{i}	9.511(3)		
Fe(2)···Fe(3)	2.916(1)	Fe(1)···Fe(4)^{i}	12.441(5)		
Fe(2)···Fe(4)	3.446(3)	Fe(2)···Fe(2)^{i}	11.902(4)		
Fe(3)···Fe(4)	3.321(3)	Fe(2)···Fe(3)^{i}	11.255(5)		

Symmetry code: i = $-x$, $1-y$, $-z$.

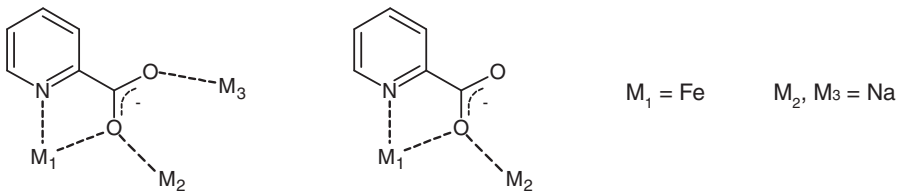

$3.2_{12}1_31_1$ 2.201

Scheme 1. Coordination modes of picolinate found in complex **3**. The numbers below each bonding mode refer to the Harris notation.

both sodium atoms. This fairly unique disposition of eight bridging carboxylate groups around a $[Fe_4Na_2(\mu_4\text{-}O)_2]^{10+}$ core has been previously observed in the structures of $[Fe_4Na_2O_2(O_2CMe_3)_{10}(MeCN)(Me_2CO)]$ and $[Fe_4Na_2O_2(O_2CMe_3)_{10}(HO_2CMe_3)_2]\cdot 4CH_2Cl_2$ [25]. An additional difference with **1** is that the terminal picolinate bridges the wingtip Fe(4) with Na(2) in a 2.201 mode. Coordination around Na(2) is completed by one water molecule leading to a distorted trigonal bipyramidal geometry, with O(90) from pic and O(20) and O(40) from two benzoates equatorial, and O(3w) and μ_4-O(2) axial donor atoms. Unlike Na(2), a highly distorted six-coordinated geometry at Na(1) is provided by oxygen donor atoms O(21) and O(41) from two benzoates, O(1w) from a water molecule, O(1) from the μ_4-O^{2-} ion and O(100) and O(101) from the two picolinates that join both subunits.

Most of the free solvent is located in the intermolecular space between the $\{Fe_8Na_4\}$ units. Atoms O(4w), O(5w), O(6w) and O(7w) undergo a major disorder, evidenced by the increase of their U_{ij} parameters, which is a reasonable consequence of the presence of conformational disorder.

3.3. Electrochemical properties

Fig. 4 shows the voltammetric profile of Au-*pc* in solutions of **1** and **2** in MeCN obtained at the potential scan rate $v = 0.050$ V s^{-1}. From the obtained profiles it was possible to assess the presence of four couples related to the Fe^{III}/Fe^{II} pair of the iron atoms in the core of both compounds that were better resolved working at low v values. These four couples could be paired in two groups of two couples each.

The first group of two couples was detected in the two analyzed complexes showing almost the same features. The first couple was located at $E'^{\circ} = -0.31$ V with $\Delta E_p = 0.11$ V, where ΔE_p represents the anodic to cathodic potential peak separation ($E_{pa} - E_{pc}$), and E'° corresponds to the formal redox potential of the couple calculated as $(E_{pa} + E_{pc})/2$. The process was controlled by the slow transference of the electron, with a slope of 30 mV/decade for the cathodic peak potential, in accordance with a transfer coefficient equal to 0.5 for a one-electron exchange process. The second couple of this group had $E'^{\circ} = -0.45$ V with $\Delta E_p = 0.14$ V, and E_p independent of v.

For **1**, the second group of two couples was detected at $E'^{\circ} = -0.82$ V and $E'^{\circ} = -0.92$ V with $\Delta E_p = 0.06$ V in both cases, showing a slow electron transfer process with a slope of 24 mV/decade for the cathodic potential peak of the second step. For the case of **2**, the second group involves one couple at $E'^{\circ} = -0.85$ V with $\Delta E_p = 0.06$ V, for a slow transfer electron process with a slope of 22 mV/decade for the cathodic potential peak. The other couple had $E'^{\circ} = -0.94$ V, $\Delta E_p = 0.06$ V, and showed a slow electron

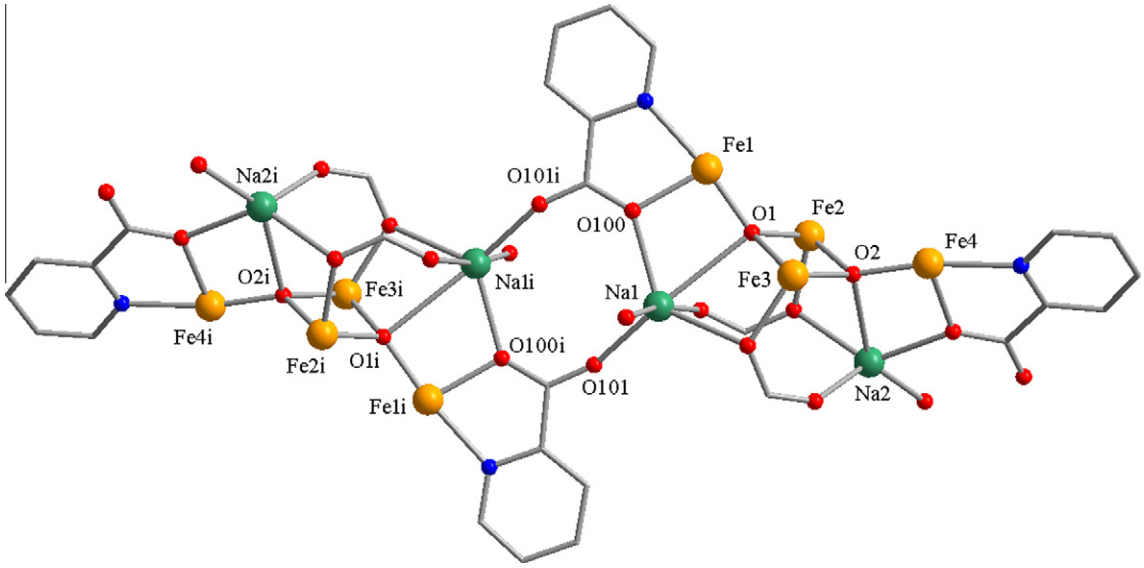

Fig. 3. Core structure of **3**.

transfer process with a slope of 18 mV/dec for both anodic and the cathodic potential peaks. All the processes involved the diffusion of the electroactive species towards the electrode surface, in accordance with the observed E_p versus $v^{1/2}$ linear adjust.

The evaluation of the solutions at the end of the measurements for both complexes showed the presence of a red-brown precipitate. This could be attributed to the formation of iron hydroxide. In this case, a further signal was observed (not shown in Fig. 4) with $E'^{\circ} = -0.65$ V, $\Delta E_p = 0.01$ V and E_p independent of v in accordance with a quasi reversible adsorption process [26].

3.4. Magnetic properties

The magnetic properties of **1** and **3** under the form of χ_M versus T plot (χ_M being the molar paramagnetic susceptibility) are shown in Fig. 5. The thermal variation of χ_M shows a decrease on cooling to reach a broad minimum at 15 K, and then rises again. In turn, the corresponding $\chi_M T$ values of 2.6 (**1**) and 5.9 $cm^3\ mol^{-1}\ K$ (**3**) at room temperature, are significantly lower than the theoretical values for four and eight non-interacting $S = 5/2$ ions (17.5 $cm^3\ mol^{-1}\ K$ and 35.0 $cm^3\ mol^{-1}\ K$), respectively, indicating the presence of dominant antiferromagnetic interactions (Fig. 6). Upon cooling, $\chi_M T$ decreases monotonically to reach a plateau near 0.007 (**1**) and 0.015 $cm^3\ mol^{-1}\ K$ (**3**) below 15 K. This analogous behavior observed for **1** and **3**, agrees with an $S = 0$ ground state with a small fraction of a paramagnetic impurity for both compounds.

The magnetic exchange interaction in the basic $[Fe_4O_2]^{8+}$ core structure can be described with the isotropic spin Hamiltonian of Eq. (2) [6b,27]:

$$\boldsymbol{H} = -J_{wb}(\boldsymbol{S}_A\boldsymbol{S}_C + \boldsymbol{S}_A\boldsymbol{S}_D + \boldsymbol{S}_B\boldsymbol{S}_C + \boldsymbol{S}_B\boldsymbol{S}_D) - J_{bb}(\boldsymbol{S}_A\boldsymbol{S}_B) \quad (2)$$

In this equation only two exchange constant were considered, J_{wb} between all wingtip-body Fe_2 pairs and J_{bb} between body-body atoms, based on symmetry considerations and in order to avoid overparametrization. The labeling scheme for the $\boldsymbol{S}_i\boldsymbol{S}_j$ terms is shown in Scheme 2.

When the magnetic data for compound **1** were analyzed through the theoretical expressions for the magnetic susceptibility derived from Eq. (2), a very good fit was achieved with the parameters $J_{wb} = -81.5(2)\ cm^{-1}$, $J_{bb} = -20(4)\ cm^{-1}$, and $\rho = 3.95(5) \times 10^{-4}$ (ρ is the molar fraction of noncoupled species). The g factor was fixed at 2.0, as would be expected for isotropic high-spin Fe^{III} ions [6b]. The goodness of the fit is reflected in the value of $R = 1.49 \times 10^{-4}$, the agreement factor, defined as $\sum_i[(\chi_m T)_{obs}(i) - (\chi_m T)_{calc}(i)]^2/\sum_i[(\chi_m T)_{obs}(i)]^2$.

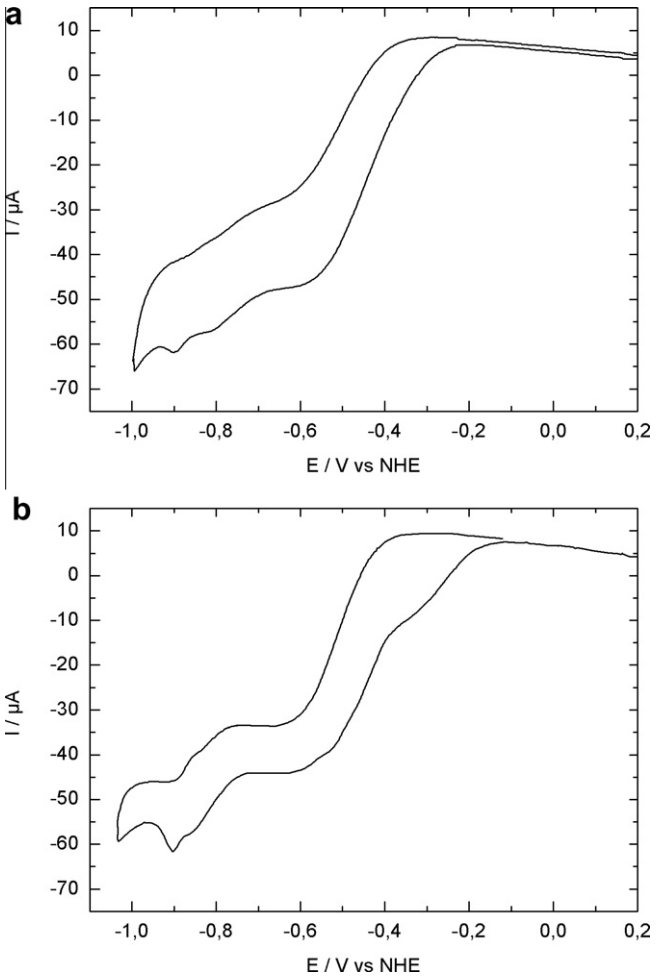

Fig. 4. Voltammetric profile of Au-pc in 1 mM solution of **1** (a) and **2** (b) in 0.04 M NEt_4ClO_4 in MeCN.

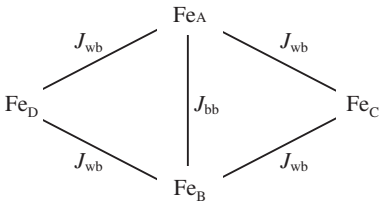

Scheme 2. Exchange interaction model used for $[Fe_4O_2]^{8+}$ core in **1**.

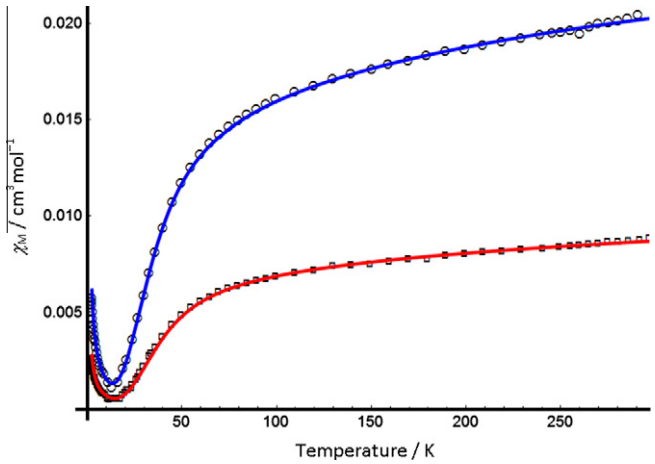

Fig. 5. Plot of the molar magnetic susceptibility vs temperature for **1** (squares) and **3** (circles). The solid lines correspond to the best theoretical fit (see the text for details).

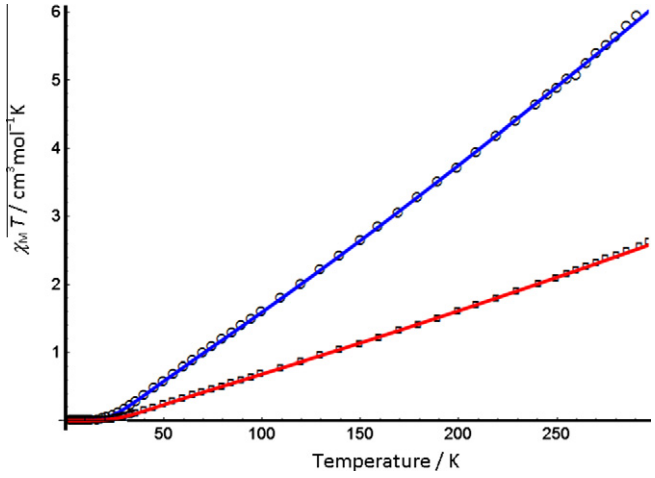

Fig. 6. Thermal dependence of $\chi_M T$ for **1** (squares) and **3** (circles). The solid lines correspond to the best theoretical fit (see the text for details).

Additionally, we performed DFT calculations of the energy for different spin arrangements in order to determine the theoretical values for J_{wb} and J_{bb} in **1**, following the well established procedure described in [28]. Only three calculations are needed in order to get completeness in the determination of the two exchange constants, but we followed with another two spin arrangements in order to get optimized values for both constants. According to the data presented in Table 5, the refined parameters are $J_{wb} = -92(3)\,cm^{-1}$ and $J_{bb} = -22(9)\,cm^{-1}$. These values agree quite well with the ones obtained from magnetic susceptibility measurements and also show the higher uncertainty in the J_{bb} parameter that was previously noted and discussed for other

Table 5
Calculated total energy for the five evaluated spin arrangements, in reference to the ground state solution.

Fe_A	Fe_B	Fe_C	Fe_D	Normalized total energy (eV)
↑	↑	↑	↑	1.090
↑	↑	↑	↓	0.499
↑	↑	↓	↓	0.000
↑	↓	↑	↓	0.447
↓	↑	↑	↑	0.462

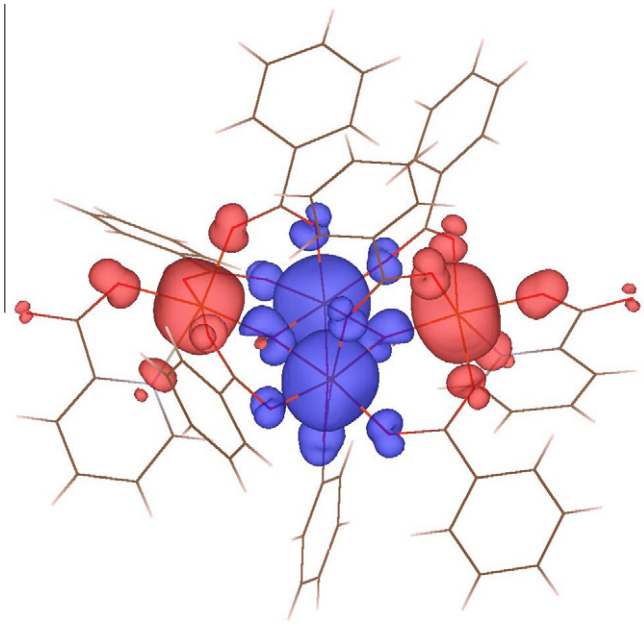

Fig. 7. Spin density map for the ground state $S = 0$ of $[Fe_4O_2(O_2CPh)_7(pic)_2]^-$ ion. Blue and red indicates negative and positive spin density, respectively. (For interpretation of the references in colour in this figure legend, the reader is referred to the web version of this article.)

similar systems [6b]. These results are also consistent with the reported exchange coupling constants of other $\{Fe^{III}_4\}$ complexes with similar spin topologies [5c] and with previous theoretical calculations [28].

In all the cases the calculated spin density over the metal ions corresponded to 3.9 μ_B, which is lower than the expected for $S = 5/2$ Fe^{III} ions. The reason for these low magnetic moments is due to the spin-delocalization in the surrounding oxygen atoms. This feature, as well as the isotropy of the spin density of Fe^{III} ions can be seen in Fig. 7.

Finally, the same spin Hamiltonian was used to described the magnetic behavior of **3**, assuming that the separation between Fe(1) and Fe(1i) in the structure precludes any significant interaction between them. In this approach, the $\{Fe_8Na_4\}$ core was simply regarded as the sum of two equivalent magnetically isolated $\{Fe_4\}$ subunits. Then, an excellent fit was accomplished with the parameters $J_{wb} = -73.3(2)\,cm^{-1}$, $J_{bb} = -29(2)\,cm^{-1}$, and $\rho = 4.39(5) \times 10^{-4}$ ($R = 4.91 \times 10^{-5}$).

3.5. Concluding remarks

Three Fe^{III}-oxo carboxylate/picolinate clusters have been prepared by reaction of "basic iron carboxylates" with sodium picolinate in MeCN. We have found that different precursor complexes $[Fe_3O(O_2CR)_6(H_2O)_3]^+$ produces analogous tetranuclear complexes of formula $(PPh_4)[Fe_4O_2(OOCR)_7(pic)_2]$ in the presence of PPh_4Cl, with R = Ph (**1**) so as Bu^t (**2**). However, a higher nuclearity

compound $[Fe_8Na_4O_4(O_2CPh)_{16}(pic)_4(H_2O)_4]$ (**3**) could be isolated when Na^+ is the unique cation in the reaction medium. Compound **1** contains the common $[Fe_4(\mu_2\text{-}O)_2]^{8+}$ core. In turn, compound **3** exhibit a $[Fe_8Na_4(\mu_4\text{-}O)_4]^{20+}$ core, where two picolinate anions coordinate in a fairly uncommon bridging mode. Both of them have been found to possess $S = 0$ ground states. Mass spectrometry and electrochemical studies suggested that the molecular structures of the anions in **1** and **2** are probably retained in MeCN. Both species are relatively easy to reduce, in a successive process which involves the four iron atoms. This is of great interest for the synthesis of partially reduced $Fe^{II}_xFe^{III}_{4-x}$ structurally related compounds, for which $S > 0$ ground states can be expected.

Acknowledgements

This work was supported by DICyT (PDT Project #63/337), CSIC (Project #402) and PEDECIBA-Química (Uruguay), CNPq, CAPES and FAPERJ (Brazil). X-ray data collection (compound **3**) and partial structure refinement was carried out during the "2008 ACA Summer Course" (Indiana University of Pennsylvania). L.A. is indebted to ACA for financial support and to ANII (Agencia Nacional de Investigación e Innovación) for a scholarship. The authors also thank Lic. Lorena Martínez for her collaboration in structure refinements and Dra. María Alejandra Rodríguez for mass spectrum measurements (Polo Tecnológico de Pando, Facultad de Química).

Appendix A. Supplementary material

CCDC 791250 and 791251 contain the supplementary crystallographic data for complexes **1** and **3**, respectively. These data can be obtained free of charge from The Cambridge Crystallographic Data Centre via www.ccdc.cam.ac.uk/data_request/cif. Supplementary data associated with this article can be found, in the online version, at doi:10.1016/j.ica.2011.02.021.

References

[1] D.M. Kurtz Jr., Chem. Rev. 90 (1990) 585;
(b) H. Toftlund, K.S. Murray, P.R. Zwack, L.F. Taylor, O.P. Anderson, J. Chem. Soc., Chem. Commun. (1986) 191;
(c) S.J. Lippard, Angew. Chem., Int. Ed. Engl. 27 (1988) 344.
[2] E.C. Theil, Annu. Rev. Biochem. 56 (1987) 289 (and references therein);
(b) K.L. Taft, G.C. Papaefthymiou, S.J. Lippard, Science 259 (1993) 1302.
[3] A.L. Barra, A. Caneschi, A. Cornia, F. Fabrizi de Biani, D. Gateschi, C. Sangregorio, R. Sessoli, L. Sorace, J. Am. Chem. Soc. 121 (1999) 5302;
(b) S. Parsons, G.A. Solan, R.E.P. Winpenny, C. Benelli, Angew. Chem., Int. Ed. Engl. 35 (1996) 1825;
(c) L.F. Jones, E.K. Brechin, D. Collison, M. Helliwell, T. Mallah, S. Piligkos, G. Rajaraman, W. Wernsdorfer, Inorg. Chem. 42 (2003) 6601;
(d) A.M. Ako, V. Mereacre, Y. Lan, W. Wernsdorfer, R. Clérac, C.E. Anson, A.K. Powell, Inorg. Chem. 49 (2010) 1.
[4] (a) R. Sessoli, D. Gatteschi, A. Caneschi, M.A. Novak, Nature 365 (1993) 141;
D. Gatteschi, R. Sessoli, A. Cornia, Chem. Commun. (2000) 725.
[5] (a) O. Khan, Chem. Phys. Lett. 265 (1997) 109;
(b) C. Cañada-Vilalta, T.A. O'Brien, E.K. Brechin, M. Pink, E.R. Davidson, G. Christou, Inorg. Chem. 43 (2004) 5505;
(c) T.C. Stamatatos, A.K. Boudalis, Y. Sanakis, C.P. Raptopoulou, Inorg. Chem. 45 (2006) 7372.
[6] See for example: J.B. Vincent, J.C. Huffman, G. Christou, Q. Li, M.A. Nanny, D.N. Hendrickson, H. Fong, R.H. Fish, J. Am. Chem. Soc. 110 (1988) 6898;
(b) J.K. McCusker, J.B. Vincent, E.A. Schmitt, M.L. Mino, K. Shin, D.K. Coggin, P.M. Hagen, J.C. Huffman, G. Christou, D.N. Hendrickson, J. Am. Chem. Soc. 113 (1991) 3012;
(c) E.J. Seddon, J.C. Huffman, G. Christou, J. Chem. Soc., Dalton Trans. (2000) 4446;
(d) A.K. Boudalis, N. Lalioti, G.A. Spyroulias, C.P. Raptopoulou, A. Terzis, A. Bousseksou, V. Tangoulis, J. Tuchagues, S.P. Perlepes, Inorg. Chem. 41 (2002) 6474.
[7] M.W. Wemple, D.K. Coggin, J.B. Vincent, J.K. McCusker, W.E. Streib, J.C. Huffman, D.N. Hendrickson, G. Christou, J. Chem. Soc., Dalton Trans. (1998) 719.
[8] M.A. Kiskin, A.A. Sidorov, G.G. Aleksandrov, Y.G. Shvedenkov, V.N. Ikorskii, V.M. Novotortsev, I.L. Eremenko, I.I. Moiseev, Russ. Chem. Bull. Int. Ed. 54 (2005) 2211.
[9] A.K. Boudalis, Y. Sanakis, F. Dahan, M. Hendrich, J. Tuchagues, Inorg. Chem. 45 (2006) 443.
[10] E. Libby, J.K. McCusker, E.A. Schmitt, K. Folting, D.N. Hendrickson, G. Christou, Inorg. Chem. 30 (1991) 3486.
[11] R.F. Weinland, A. Herz, Ber. Dtsch. Chem. Ges. 45 (1912) 2662.
[12] Molecular Structure Corporation, MSC/AFC Diffractometer Control Software, MSC, 3200 Research Forest Drive, The Woodlands, TX 77381, USA, 1988.
[13] G.M. Sheldrick, Acta Crystallogr., Sect. A 64 (2008) 112.
[14] L.J. Farrugia, J. Appl. Crystallogr. 32 (1999) 837.
[15] A.L. Spek, Acta Crystallogr., Sect. A 46 (1990) C-34.
[16] P. Hohenberg, W. Kohn, Phys. Rev. 136 (1964) B864.
[17] W. Kohn, L.J. Sham, Phys. Rev. 140 (1965) A1133.
[18] P. Ordejón, E. Artacho, J.M. Soler, Phys. Rev. B 53 (1996) R10441.
[19] D. Sánchez-Portal, P. Ordejón, E. Artacho, J.M. Soler, Int. J. Quantum Chem. 65 (1997) 453.
[20] J.M. Soler, E. Artacho, J.D. Gale, A. García, J. Junquera, P. Ordejón, D. Sánchez-Portal, J. Phys.: Condens. Matter 14 (2002) 2745.
[21] N. Troullier, J.L. Martins, Phys. Rev. B 43 (1991) 1993.
[22] (a) J.P. Perdew, K. Burke, M. Ernzerhof, Phys. Rev. Lett. 77 (1996) 3865;
(b) J.P. Perdew, K. Burke, M. Ernzerhof, Phys. Rev. Lett. 78 (1997) 1396.
[23] W. Henderson, J.S. McIndoe, Mass Spectrometry of Inorganic, Coordination and Organometallic Compounds: Tools–Techniques–Tips, John Wiley and Sons Ltd., Chichester, England, 2005.
[24] Harris notation describes the binding mode as $[X.Y_1Y_2Y_3\ldots Y_n]$, where X is the overall number of metals bound by the whole ligand, and each value of Y refers to the number of metal atoms attached to the different donor atoms. See: R.A. Coxall, S.G. Harris, D.K. Henderson, S. Parsons, P.A. Tasker, R.E.P. Winpenny, J. Chem. Soc., Dalton Trans. (2000) 2349.
[25] R. Çelenligil-Çetin, R.J. Staples, P. Stavropoulos, Inorg. Chem. 30 (2000) 5838.
[26] G. Milazzo, S. Caroli, Tables of Standard Electrode Potentials, John Wiley and Sons Ltd., New York, 1975;
A.J. Bard, L.R. Faulkner, Electrochemical Methods, John Wiley and Sons Ltd., New York, 1980.
[27] J.B. Vincent, C. Christmas, H.R. Chang, Q. Li, P.D.W. Boyd, J.C. Huffman, D.N. Hendrickson, G. Christou, J. Am. Chem. Soc. 111 (1989) 2086.
[28] T. Cauchy, E. Ruiz, S. Alvarez, J. Am. Chem. Soc. 128 (2006) 15722.